Biochemistry and Biophysics Reports 5 (2016) 379–387

Contents lists available at ScienceDirect

Biochemistry and Biophysics Reports

journal homepage: www.elsevier.com/locate/bbrep

Comparative proteomic analysis of growth hormone secretagogue A233 treatment of murine macrophage cells J774A.2 indicates it has a role in antiviral innate response ☆

Rebeca Martínez [a,1], Teresa Núñez de Villavicencio-Díaz [b,1], Aniel Sánchez [b], Yassel Ramos [b], Jesús Noda Ferro [b], Lázaro Gil González [c], Milagros Méndez [d], Elsa Rodríguez [a], Ernesto Marcos [c], Belinda Sánchez [e], Yordanka Masforrol [f], Hilda Garay [f], Fernando Albericio [g], Lisset Hermida [c], Luis Javier González [b], Eva Vonasek [d], Mario P Estrada [a,*], Vladimir Besada [b,*]

[a] Animal Biotechnology Division, Center for Genetic Engineering and Biotechnology, P.O. Box 6162, Havana 10600, Cuba
[b] Department of Systems Biology, Center for Genetic Engineering and Biotechnology, Havana, Cuba
[c] Vaccines Division, Center for Genetic Engineering and Biotechnology, Havana, Cuba
[d] Proteomics Unit, Department of Structural Biology, Venezuelan Institute for Scientific Research, PO Box 20632, Caracas, Venezuela
[e] Center for Molecular Immunology, Havana, Cuba
[f] Synthetic Peptides Group, Physics and Chemistry Department, Center for Genetic Engineering and Biotechnology, Havana, Cuba
[g] Department of Organic Chemistry, University of Barcelona, 08028 Barcelona, Spain

ARTICLE INFO

Article history:
Received 23 June 2015
Received in revised form
18 December 2015
Accepted 12 January 2016
Available online 14 January 2016

Keywords:
Comparative proteomics
Growth Hormone Secretagogue
ROS production
Antiviral activity

ABSTRACT

Background: Growth hormone secretagogues (GHS), among other factors, regulate the release of GH. The biological activity of the secretagogue peptide A233 as a promoter of growth and innate immunity in teleost fish has previously been demonstrated, but its role in the immune system of mammals is not well understood.
Methods: The effect of the peptide was investigated in J774A.2 macrophage cells using a comparative proteomics approach after 6 and 12 h of peptide stimulation.
Results: The functional analysis of differentially modulated proteins showed that A233 peptide treatment appears to promote activation and ROS-dependent cytotoxic functions in macrophages and enhanced expression of antiviral protein complexes such as MAVS. In accordance with this hypothesis, we found that A233 treatment enhanced superoxide anion production and the IFN-γ level in J774A.2 cells and mouse splenocytes, respectively, and reduced viral load in a dengue virus mouse model of infection.
Conclusions: The growth hormone secretagogue A233 peptide promotes activation of ROS-dependent cytotoxic functions and exerts immunomodulatory effects that enable an antiviral state in a dengue virus mouse model.
General Significance: The increase of IFN-γ level and the differential modulation of antiviral proteins by the A233 peptide suggest that the molecule could activate an innate immune response with a possible further impact in the treatment of acute and chronic diseases.

1. Introduction

Growth hormone secretagogues (GHS) such as ghrelin induce an array of effects in different types of organisms [1]. The A233 decapeptide is a novel synthetic GHS obtained from a massive docking experiment performed against a molecular model of the GHS receptor. So far, studies have demonstrated an impact of peptide treatment on growth, immune system function, and antioxidant defense in tilapia fish [2].

The role of ghrelin in immune cell activation includes the

Abbreviations: DENV, dengue virus; GHRP-6, growth hormone releasing peptide-6; [D-Lys3]-GHRP-6t, ghrelin receptor antagonist; GHS, growth hormone secretagogue; IFN-γ, interferon gamma; LPS, lipopolysaccharide; $O_2^{\bullet -}$, superoxide anion; RNS, reactive nitrogen species; ROS, reactive oxygen species

☆Author Contributions: the manuscript was written through contributions of all authors. All authors have given approval for the final version of the manuscript.

* Corresponding authors.
E-mail addresses: mario.pablo@cigb.edu.cu (M. Estrada), vladimir.besada@cigb.edu.cu (V. Besada).

[1] These authors contributed equally

http://dx.doi.org/10.1016/j.bbrep.2016.01.008

release of pro- and anti-inflammatory cytokines via different signaling pathways [3]. For example, murine RAW 264.7 macrophages express both ghrelin and GHS receptors. Treatment of these cells with exogenous ghrelin decreases LPS-dependent NF-κB activation and subsequent IL-1β and TNF-α production (pro-inflammatory cytokines), while it increases IL10 (anti-inflammatory cytokine) levels through the p38MAPK pathway [4]. GHS also stimulates oxidized LDL uptake by macrophages and PPAR-γ signaling, both being functions associated with the pathogenesis of cardiovascular diseases such as atherosclerosis [5,6].

Macrophage activation is a complex process that involves significant changes in metabolism and gene expression [7]. Two main classifications exist for activated macrophages: M1 (classically activated) and M2 (alternatively activated). This classification represents extremes of functional polarization [8]. M1 polarization of macrophages occurs in the presence of interferon-γ (IFN-γ) and lipopolysaccharide (LPS), whereas exposure to interleukins IL-4 and IL-13 induces M2 polarization. Classically activated macrophages display strong anti-pathogen and antitumor activity, inducing an increase of pro-inflammatory cytokines, reactive oxygen species (ROS) and reactive nitrogen species (RNS). Alternatively activated macrophages function in tissue remodeling, tumor progression, immunoregulation, inflammation reduction, and parasite elimination [9].

The evidence of immune system stimulation by the A233 peptide in teleost fish prompted us to investigate this process in mouse macrophages to obtain a better understanding of the effect at the molecular level. This work explores the proteome of J774A.2 mouse macrophage cells stimulated by treatment with A233 for 6 or 12 h. Differentially modulated proteins were found by quantitative comparison using 4-plex iTRAQ derivatization. The functional analysis of the differentially modulated proteins in the context of macrophage activation suggested that peptide treatment induces M1 polarization. To investigate these events, we measured the levels of $O_2^{\bullet-}$ (superoxide anion) and IFN-γ, two key players in classical macrophage activation. A significant increase of both molecules was found, which reflects an enhancement in ROS-dependent cytotoxicity and the induction of an antiviral state in treated macrophages and splenocytes, respectively.

Data obtained by our proteomics study revealed the up-regulation of proteins related to inflammation and antiviral activity, such as mitochondrial antiviral signaling protein (MAVS), which plays an important role in antiviral innate immunity as well as cell death. Given the importance of these findings, the antiviral response induced by the A233 peptide was studied in a mouse model of intracranial dengue virus infection. To our knowledge, this is the first time that antiviral activity in vivo produced by a secretagogue growth hormone has been reported.

2. Materials and methods

2.1. Peptide synthesis

The decapeptide A233 (GKFDLSPEHQ), with a lactam bond between side chain functional groups of Lys^2 and Asp^4, was manually synthesized on Fmoc-AM-PEG-PS resin (substitution level: 0.18 mmol/g) using the Fmoc/tBu strategy. All side-chains were protected with TFA-labile groups and the side-chain protections used for Lys and Asp were allyloxycarbonyl (Alloc) and allyl (All), respectively. Removal of the Fmoc group was carried out with 20% piperidine in DMF and the Fmoc-amino acids were coupled using DIC/HOBt activation. Once the complete peptide sequence had been assembled, and maintaining the Fmoc-Nα-protection, the Alloc-All groups were removed by treatment with phenylsilane and tetrakistriphenylphosphine palladium (0). The lactam bond was obtained by treatment of the peptide-resin with PyBOP/DIEA in DMF. Side-chain deprotection and cleavage from the resin were carried out with TFA-H_2O-TIS (95:2.5:2.5 v/v). The peptide was purified by reversed-phase high performance liquid chromatography (RP-HPLC). The A233 peptide was obtained with purity higher than 95%, as estimated by analytical RP-HPLC. The identity of the A233 was verified by ESI-MS analysis. The experimental (1137.58 Da) and calculated (1137.56 Da) monoisotopic molecular mass agreed, considering the formation of the lactam bond previously described. The ESI-MS/MS spectrum of the doubly-charged ion of A233 peptide (*m/z* 569.79, 2+) was acquired to obtain structural evidence of the lactam bond formation between Lys^2 and Asp^4 from the backbone and internal fragment ions. The positive control GHRP-6 (Lipotec, Barcelona, Spain) and its antagonist [D-Lys^3]-GHRP-6 (Sigma), both lyophilized, were reconstituted in PBS for use in in vitro and in vivo assays.

2.2. Reverse phase chromatography.

A233 peptide was analyzed on an AKTA 100 (GE Healthcare, USA) HPLC system. Analytical analysis was accomplished in a reverse-phase (RP) C18 analytical column (4.6 × 150 mm, 5 μm) (Vydac, USA). To assess the peptide purity, the column was equilibrated in 95% solution A, then a linear gradient from 5% to 60% solution B, over 35 min, was used keeping a flow rate of 0.8 mL/min. The solutions A and B used in the purification were 0.1% of TFA in water, and 0.05% of TFA in pure acetonitrile, respectively. Chromatograms were acquired at 226 nm, using the UNICORN 4.11 (GE Healthcare, USA) software package for data processing of the RP-HPLC chromatograms. The semipreparative purification was performed on a LaChrom (Merck-Hitachi, Germany) HPLC system. Separation was achieved using an RP C18 preparative column (Vydac, 25 × 250 mm, 25 μm). A linear gradient from 15% to 45% of solvent B over 50 min and a flow rate of 5 mL/min were used. Solvents A and B are composed of 0.1% (v/v) of TFA in water and 0.05% (v/v) of TFA in acetonitrile, respectively. Detection was monitored at 226 nm.

2.3. Mass spectrometric analysis.

ESI-MS analysis was performed in a hybrid quadrupole-time-of-flight (QTOF-2™) tandem mass spectrometer (Waters, Milford, MA, USA) equipped with a Z-nanospray ion source. Capillary and cone voltages were set to 900 and 35 V, respectively. A 5 μL aliquot of the peptide purified by RP-HPLC was loaded into a glass capillary coated with conductive material (New Objective, Woburn, MA, USA). The tip of the capillary was gently broken, while slightly pressurized with nitrogen, in order to get a stable spray during the measurement. The TOF and MCP were operated at 2.2 kV and 9 kV, respectively. The source was heated at 90 °C. The doubly-charged ion of the A233 peptide (*m/z* 569.79, 2+) was selected in the first quadrupole and fragmented inside the collision cell operated at collision energy of 35 eV to obtain an MS/MS spectrum with structural information. Ultrapure Argon (Gases Industriales, Cuba) was used as a collision gas. Data acquisition and processing were performed with the MassLynx (v. 4.0) software package (Waters, USA).

2.4. Growth conditions for J774.2 cells

The J774A.2 cell line was obtained from ECACC (85011428 Sigma). The cells were cultured as monolayers in Dulbecco's Modified Essential Medium (DMEM) F12 supplemented with 20% fetal bovine serum (FBS), 100 mg/mL penicillin/streptomycin, and 2 mM L-glutamine (Mediatech, Inc., Herndon, VA) at 37 °C in a humidified atmosphere of 5% CO_2. The cultured cells were grown

to 70–80% confluence in 75 cm^2 flasks for preparation of samples that were used in further analyses.

2.5. Superoxide production by J774.2 cells

Superoxide anion production was measured in J774.2 cells by the reduction of nitro blue tetrazolium (NBT; Sigma, USA) following the procedure described by Yada et al. [10].

2.6. IFN-γ production in mouse splenocytes

Mouse splenocytes were obtained in aseptic conditions, and erythrocytes were lysed by adding 0.83% NH_4Cl solution. Cells were washed twice with PBS containing 2% FBS (PAA Laboratories, ON, Canada) and resuspended at 2×10^6 cells/mL in RPMI 1640 medium (Sigma Aldrich, USA) supplemented with 100 U/mL penicillin, 100 μg/mL streptomycin (Gibco, UK), 2 mM glutamine (Gibco), 5×10^{-5} M 2-mercaptoethanol (Sigma, USA) and 5% FBS. Finally, 2.5×10^5 cells per well were cultured in 96-well round-bottom plates with the peptides at a final concentration of 10 μg/mL. Concanavalin-A (Sigma) was used as a positive control. In all experiments, three wells were plated for each antigen. After 4 days of culture, culture supernatants were collected and stored at −20 °C. IFN-γ was determined by ELISA (as recommended by Mabtech) in duplicate samples from culture supernatants.

2.7. Reduction and S-alkylation

Tubes containing proteins from each of the three experimental conditions (control at 0 h, and 6 h or 12 h of A233 treatment) received 45 μL of 50 mM Hepes, 2 M GuCl, pH 8.5 and the mixtures were reduced by adding dithiothreitol (DTT) to a final concentration of 10 mM and incubating the tubes for 4 h at 37 °C. The free thiol groups were alkylated by adding iodoacetamide to a final concentration of 20 mM, and allowing the reactions to proceed (in darkness) for an additional 30 min at room temperature.

2.8. Proteolytic digest

Hepes, pH 8.5 (50 mM) was added to 100 μL final volume, and proteins were digested with Lysyl-endopeptidase (Wako, Japan) using an enzyme:substrate ratio of 1:100 for 4 h at 37 °C. After digestion, the peptide mixture was diluted with water up to 0.5 mol/L guanidium hydrochloride. Sequencing grade trypsin (Promega, USA) was added to a concentration of 1:100 (enzyme: substrate), and the reaction proceeded for 16 h at 37 °C.

2.8.1. iTRAQ modification

Eighty μg of protein digest was dried and re-suspended in 30 μL of 50 mM Hepes, pH 8.5, for labeling using the iTRAQ Reagents Four-plex Kit (Applied Biosystems, USA), according to the manufacturer's protocol. Briefly, each peptide solution was labeled at room temperature for 1 h with one iTRAQ reagent vial (mass tag 114, 115 or 117) previously reconstituted with 70 μL of ethanol. The differential protein expression profiles of J774A.2 in the three conditions were analyzed in duplicate: 0 h control sample (114) and 6 h (115) and 12 h (117) of the A233 treatment. Samples with the same amount of protein, labeled with 114, 115 and 117 iTRAQ reagents, respectively, were combined into a single fraction, and the labeling reaction was stopped by evaporation in a Speed Vac (Savant, USA). The samples were desalted using RP-cartridges (RP C8, SPE Sep-Pak Light, Waters, USA) and eluted in 3 mL of 80% acetonitrile. The final solutions were dried by evaporation in a Speed Vac.

2.8.2. Fractionation of the iTRAQ-labeled peptide mixture

For *pI*-based peptide separation, a 3100 OFFGEL Fractionator (Agilent Technologies, Germany) was used with a 12-well set-up. Prior to electrofocusing, samples were desalted using a Sep-Pak C18 cartridge (Waters, USA),dried and diluted to a final volume of 3.6 mL using OFFGEL peptide sample solution. The IPG gel strips (13 cm-long) with a 3–10 linear pH range (GE Healthcare, Germany) were rehydrated for 15 min with the Peptide IPG Strip Rehydradation Solution according to the manufacturer's instructions. Then, 150 μL of sample was loaded into each well. Electrofocusing of the peptides was performed at 20 °C and 50 μA until the 20 kVh level was reached. All fractions were desalted using Stage-tips (Thermo, USA) and evaporated by centrifugation under vacuum and maintained at −20 °C. Just prior to nano-LC, the fractions were resuspended in 20 μL H_2O with 0.1% (v/v) trifluoroacetic acid.

2.8.3. LC-MS/MS analysis of iTRAQ-labeled peptides

The labeled peptides were dissolved in 0.1% formic acid solution and delivered into an RP nano-EASY column (75 μm inner diameter × 100 mm length, 3 μm particle size, C18-A2 resin; (Thermo Scientific, USA) previously equilibrated in 5% of solution A (0.1% formic acid in water). The retained peptides were eluted using a linear gradient by increasing the content of solution B (0.1% of formic acid in acetonitrile) in the mobile phase from 5% to 45% over 90 min, at 200 nL/min. The eluated peptides were analyzed in an LTQ-Orbitrap Velos MS (Thermo Fisher Scientific, USA). MS data were acquired via data-dependent acquisition, mode by selecting the twenty top-most intense signals for an automatic MS/MS analysis. For the MS spectra, the resolution was 60,000 (FWHM) at m/z 400, and the m/z range was set from 350 to 1650. Fragmentation of peptides was achieved by HCD (higher energy collisional dissociation) activation with a resolution of 7500 (FWHM), isolation width of 2 m/z units, and first mass at $m/z = 100$. Normalized collision energies (NCEs) were set to 35%.

2.8.4. Data analysis

The Mascot (version 2.3.02) search engine and UniProtKB/Swiss-Prot database (11-2011, 533 049 entries) were used for peptide and protein identification. The search space was reduced down to 16 409 entries after applying a taxonomy filter by considering only *Mus muculus* derived proteins. Mascot tolerance parameters were set to 10 ppm and 0.2 Da for precursor mass and product ion, respectively. Other parameters used were trypsin digestion with up to two missed cleavages and a fixed modification of cysteine residues (carbamidomethylation). Oxidation of methionine to sulfoxide and iTRAQ 4-plex peptide labels were used as variable modifications. A reverse decoy database was generated and joined to the target database for false discovery calculations (< 1% FDR at the peptide level was accepted). Peptides below the identity threshold (score 23) were not considered for analysis.

The data was analyzed using the corresponding statistical tools from the MASCOT Distiller software package (version 2.5.1.0). The statistical processing includes a test of normality for the distribution of peptide fold-change values. Once it has been established that the data is normally distributed then the geometric mean of these values is compared to the unit using the Student's t-test ($p = 0.05$). The MASCOT Distiller software reports as regulated proteins those with fold-change values that are statistically different from unity. If the protein fold-change values did not set to a normal distribution, or the quantification is based in one or two peptides, the p value was calculated based on the analysis of the individual peptide(s) detected in an OFFGEL fraction that has a normal distribution. The fold changes calculated for the individual proteins in the experimental conditions are expressed respect to the intensity of the ion at m/z 114 used as control of the

experiment (0 h).

2.9. Mouse experiments and viral load detection in brain

Female BALB/c (Bc, H-2^d) mice (aged 6–8 weeks) were purchased from CENPALAB (Havana, Cuba) and housed in appropriate animal care facilities during the experimental period. Mouse experiments were carried out in strict accordance with the recommendations in the Guide for the Care and Use of Laboratory Animals of the Center for Genetic Engineering and Biotechnology (CIGB), Cuba. The protocols were approved by the CIGB Committee on Ethics for Animal Experiments.

Two groups of eight mice were injected intraperitoneally on days 0, 1, 3, 4, 6 and 7 with 10 μg of peptide A233 per animal or PBS (control) without adjuvant in a final volume of 100 μL. A third group was injected with the [D-Lys^3]-GHRP6 antagonist peptide using the same schedule. As a positive control for the challenge with dengue virus (DENV), a fourth group of animals was inoculated with 10^5 plaque-forming units (pfu) of an infectious preparation of DENV-3 (H87 strain, 27 passages in mice) on day 0.

On day 8, animals were challenged with 50 LD_{50} of neuroadapted DENV-3 H87 by intracranial injection. Seven days after challenge, mice were euthanized to measure the viral load in brain as previously reported [11]. Brains were harvested and aseptically homogenized with 1 mL of PBS supplemented with 2% FBS, 100 U/mL penicillin and 100 μg/mL streptomycin. The suspensions were centrifuged for 10 min at 8000*g*, and supernatants were collected and stored at −80 °C.

For viral load measurement, 5×10^5 Vero cells/well were cultured for 24 h in six-well plates with MEM (Sigma Aldrich) supplemented with 100 U/mL penicillin, 100 μg/mL streptomycin, 2 mM glutamine, 1 mM sodium pyruvate (Gibco, UK), and 2% FBS. Cells were infected with different dilutions of the infected brain supernatants in MEM medium supplemented with 1% FBS. After infection (4 h at 37 °C and 5% CO_2), the overlay medium was added (3% carboxymethylcellulose), and the plates were incubated at 37 °C and 5% CO_2 for 4 days. Infected cells were visualized by immunofocusing. Briefly, the cells were fixed with 4% formalin for 1 h, washed twice with PBS, and then incubated in PBS-1% Triton X-100 for 15 min. After permeabilization, blocking buffer (PBS supplemented with 10% FBS) was added to each well for 30 min at room temperature. After blocking, the cells were incubated with monoclonal antibody 4G2 (which recognizes the envelope protein of DENV) at 1 μg/mL (in PBS and 1% FBS) for 1 h at room temperature. After two washes with PBS, polyclonal anti-mouse IgG-HRP (Sigma Aldrich, USA) was added at a dilution of 1:2000 (in PBS and 1% FBS) and incubated for 1 h at room temperature. The cells were then washed twice with 50 mM Tris, pH 7.4, and a substrate solution of 0.5 mg/mL diaminobenzidine, 0.2 mg/mL $CaCl_2$, and 9 mg/mL NaCl in 50 mM Tris, pH 7.4, was added to each well. The plates were left on a shaker for 30 min until clear foci were visible for subsequent counting. The detection limit was 10 pfu/mL.

2.10. Statistical analysis

For statistical analysis, GraphPad Prism version 5.0 for Windows (GraphPad Software, San Diego, CA) was used. The normal distribution of data was analyzed with D'Agostino Pearson's test and the variance homogeneity with Bartlett's test. When normal or transformed data showed a normal distribution, a parametric test was performed; otherwise data were analyzed with a non-parametric test. The parametric analysis of more than two groups was performed by a one-way analysis of variance, using Newman–Keuls post-test. The non-parametric analysis of more than two groups was performed using Kruskal–Wallis and Dunn multiple comparison test. In all cases *: $p < 0.05$; **: $p < 0.01$; ***: $p < 0.001$.

2.11. Bioinformatics analysis

The functional analysis of the differentially modulated proteins was performed in the context of classical macrophage activation. First, the function of the differentially modulated proteins was extracted from UniProtKB database [12] and the scientific literature. Information from the literature concerning macrophage activation and its relation with the differentially modulated proteins was explored with the information retrieval and text mining tool GoPubMed [13]. Next, an enrichment analysis of the differentially modulated proteins, at both 6 and 12 h and at each time separately, was performed based on the following biological annotations: GO biological process, GO molecular function, KEGG pathway, transcription factor binding site (TFBS), and mammalian phenotype ontology (MPO) [14]. GeneCodis [15] was used for GO annotations and KEGG pathway enrichment analyses, InnateDB [16] for TFBS enrichment analysis, and NetVenn [17] for MPO enrichment analysis. Default parameters were kept and the significance level was set at $p < 0.05$.

3. Results

The A233 peptide is a novel synthetic GHS that enhances both growth and the innate immune system in teleost fish [2]. Here we analyzed the proteome of the J774.2 macrophage cell line, stimulated with the peptide for 6 and 12 h. Limits for the fold changes were fixed in 0.60 and 1.5 order to identify down- and up-regulated expressed proteins. With this analysis we identified a total of 1384 proteins using 1% of false discovery rate. In Table 1, (Supplementary Material) the differentially expressed proteins are shadowed in gray. Three hundred thirty six proteins of which were differentially regulated after 6 h of treatment (between 78 and 258 proteins down- and up-regulated). After 12 h of treatment 280 proteins were differentially expressed (between 56 and 224 proteins down- and up-regulated).

The modulated proteins that might be relevant for the effect of A233 on macrophages after 6 and 12 h are summarized in Table 1. At six hours, 14 and 9 of these proteins were up- and down-regulated, respectively and with *p* values lower than 0.05. At 12 h 17 and 8 proteins were up- and down regulated, respectively. In Table 1 there are other proteins with fold changes that exceed these thresholds and could be potentially considered as differentially expressed but MASCOT did not calculate a p value either because the quantification is based on one or two peptides or the fold changes of the peptides used for the quantification did not have a normal distribution.

The GO biological process and KEGG pathway enrichment analyses of the differentially modulated proteins at both time points show the down-regulation of fatty-acid beta oxidation and the up-regulation of DNA repair and the inflammatory response (Fig. 1, Supplemental Table 2). These analyses at each time point separately also revealed the up-regulation of glycolysis after 6 h of treatment and the citrate cycle after 12 h, whereas they point to a down-regulation of electron transport chain at 6 h post-treatment (Fig. 1, Supplemental Table 2). Other biological processes or pathways modulated by the peptide treatment were: oxidation-reduction, response to hydrogen peroxide, activation of cysteine-type endopeptidase activity involved in apoptotic processes, and positive regulation of TNF production (Fig. 1, Supplemental Table 2). These significant enrichments suggest that peptide treatment impacts glucose and fatty acid catabolism, the oxidation-reduction process, DNA repair, apoptosis, and inflammation. Based on these findings, we further investigated the effect of A233

Table 1
Differentially modulated proteins at 6 and/or 12 h A233 peptide treatment that might be relevant for the effect on macrophages.

UniProt Acc	Gene Name	Protein name	Fold-Change treated 6 h[f]	Fold-Change treated 12 h[f]
Apoptotic process				
P63038/ CH60_MOUSE	Hspd1	60 kDa heat shock protein, mitochondrial	0.729 [c] $p=-$	*0.52 (F7)* [d] $p=0.05$
DNA damage response and repair				
Q9D1M4/ MCA3_MOUSE	Eef1e1	Eukaryotic translation elongation factor 1 epsilon-1	*1.903 (F6)* $p=0.0328$	*1.757 (F7)*[d] $p=0.0262$
P52479/ UBP10_MOUSE	Usp10	Ubiquitin carboxyl-terminal hydrolase 10	*1.881(F6)* * [d, e] $p=0.0585$	*1.84 (F6)** [d, e] $p=0.0655$
Q8R2Y9/ SOSB1_MOUSE	Nabp1	SOSS complex subunit B1	2.082 [c] $p=-$	**2.196** [a] $p=0.008648$
Q8BGW5/ RUVB2_MOUSE	Ruvbl2	RuvB-like 2	1.505* [e] $p=0.07101$	**1.686** [a] $p=0.01872$
Q9WTM5/ ASH2L_MOUSE	Ash2l	Set1/Ash2 histone methyltransferase complex subunit ASH2	2.5 [b] $p=$N/A	2.33 [b] $p=$N/A
Inflammation and anti-viral response				
Q60875/ ARHG2_MOUSE	Arhgef2	Rho guanine nucleotide exchange factor 2	**1.783** [b] $p=$N/A	**1.952** [b] $p=$N/A
P04117/ FABP4_MOUSE	Fabp4	Fatty acid-binding protein, adipocyte	1.707 *(F4)** [e] $p=0.05442$	1.3 * [e] $p=0.2302$
P20491/ FCERG_MOUSE	Fcer1g	High affinity immunoglobulin epsilon receptor subunit gamma	1.048 [b] $p=$N/A	**2.552** [a] $p=0.0044$
Q8VCF0/ MAVS_MOUSE	Mavs	Mitochondrial antiviral-signaling protein	**1.837** [b] $p=$N/A	**2.177** [b] $p=$N/A
Glycolysis				
P17710/ HXK1_MOUSE	Hk1	Hexokinase-1	**1.718** [a] $p=0.004512$	**1.52** [a] $p=0.02119$
Q3TRM8/ HXK3_MOUSE	Hk3	Hexokinase-3	**3.299** [a] $p=0.0008967$	1.857 *(F3)** [d,e] $p=0.06958$
Pyruvate metabolism				
P14152/ MDHC_MOUSE	Mdh1	Malate dehydrogenase, cytoplasmic	*2.938 (F6)* $p=0.0025$	1.118 *(F6)** [d,e] $p=0.561$
P45376/ ALDR_MOUSE	Akr1b1	Aldose reductase	**1.857** [a] $p=0.01542$	**1.311** [a] $p=0.0202$
TCA cycle				
Q8BH04/ PCKGM_MOUSE	Pck2	Phosphoenolpyruvate carboxykinase, mitochondrial	0.967 * [e] $p=0.6243$	**1.584** [a] $p=0.02746$
Q9CPQ1/ COX6C_MOUSE	Cox6c	Cytochrome c oxidase subunit 6C	**0.378** [a] $p=0.0000206$	0.701 [c] $p=-$
Q9CQ75/ NDUA2_MOUSE	Ndufa2	NADH dehydrogenase 1 alpha subcomplex subunit 2	**0.564** [a] $p=0.0006703$	**0.693** [a] $p=0.03969$
Q62425/ NDUA4_MOUSE	Ndufa4	Cytochrome c oxidase subunit NDUFA4	**0.545** [a] $p=0.0001127$	**0.799** [a] $p=0.005061$
Fatty acid metabolism				
Q99JY0/ ECHB_MOUSE	Hadhb	Trifunctional enzyme subunit beta, mitochondrial	**0.586** [a] $p=0.002993$	**0.215** [a] $p=0.04001$
Q8QZT1/ THIL_MOUSE	Acat1	Acetyl-CoA acetyltransferase, mitochondrial	**0.552** [a] $p=0.0000293$	**0.533** [a] $p=0.0000243$
Q8BH95/ ECHM_MOUSE	Echs1	Enoyl-CoA hydratase, mitochondrial	**0.547** [a] $p=0.0004425$	**0.558** [a] $p=0.000000162$
Insuline signaling				
P35821/ PTN1_MOUSE	Ptpn1	Tyrosine-protein phosphatase non-receptor type 1	**1.471** [a] $p=0.02174$	**2.196** [a] $p=0.001486$
Phospholipase				
Q8BG07/ PLD4_MOUSE	Pld4	Phospholipase D4	**1.984** [a] $p=0.006469$	**2.369** [a] $p=0.004143$
Oxidation-reduction process and response to H_2O_2				
P62715/ PP2AA_MOUSE	Ppp2cb	Serine/threonine-protein phosphatase 2A catalytic subunit beta isoform	*1.931 (F6)* [d] $p=0.0462$	**1.427** [a] $p=0.006338$
P08228/ SODC_MOUSE	Sod1	Superoxide dismutase [Cu–Zn]	**1.939** [a] $p=0.03721$	1.281*(F1)** [e] $p=0.06717$
O08709/ PRDX6_MOUSE	Prdx6	Peroxiredoxin-6	**1.811** [a] $p=0.01335$	**1.689** [a] $p=0.0002667$
Transcription				
Q99N69/ LPXN_MOUSE	Lpxn	Leupaxin	**2.148** [a] $p=0.04064$	1.505* [e] $p=0.2182$
Q6A068/ CDC5L_MOUSE	Cdc5l	Cell division cycle 5-like protein	1.9 [c] $p=-$	**2.021** [a] $p=0.001067$
Q9CWL8/ CTBL1_MOUSE	Ctnnbl1	Beta-catenin-like protein 1	**2.431** [a] $p=0.01294$	**1.755** [a] $p=0.04733$
RNA splicing				
Q61656/ DDX5_MOUSE	Ddx5	Probable ATP-dependent RNA helicase DDX5	*1.784 (F6)* [d] $p=0.0705$	*1.708 (F6)* [d] $p=0.0709$
Q922V4/ PLRG1_MOUSE	Plrg1	Pleiotropic regulator 1	**1.687** [a] $p=0.01822$	**2.074** [a] $p=0.03083$

Table 1 (*continued*)

UniProt Acc	Gene Name	Protein name	Fold-Change treated 6 h[f]	Fold-Change treated 12 h[f]
Q8R149/ BUD13_MOUSE	Bud13	BUD13 homolog	**2.475** [b] p=N/A	**1.916** [b] p=N/A
Q9QYS9/ QKI_MOUSE	Qki	Protein quaking	**1.907** [b] p=N/A	**1.853** [b] p=N/A
Ribosome and ribosome biogenesis				
Q99N95/ RM03_MOUSE	Mrpl3	39S ribosomal protein L3, mitochondrial	**0.495** [a] p=0.00000436	**0.509** [a] p=0.00000175
Intracellular protein transport				
Q9JKC8/ AP3M1_MOUSE	Ap3m1	AP-3 complex subunit mu-1	**0.532** [b] p=N/A	**0.377** [b] p=N/A
Protein folding and degradation				
O70591/ PFD2_MOUSE	Pfdn2	Prefoldin subunit 2	**1.605** [a] p=0.01261	**1.517** [a] p=0.02322
P61082/ UBC12_MOUSE	Ube2m	NEDD8-conjugating enzyme Ubc12	**2.066** [a] p=0.001301	1.675 * p=0.1142
Q922Y1/ UBXN1_MOUSE	Ubxn1	UBX domain-containing protein 1	2.208 [c] p= —	**1.783** [a] p=0.01412
P97821/ CATC_MOUSE	Ctsc	Dipeptidyl peptidase 1	**2.123** [a] p=0.001438	**2.056** [a] p=0.004243
Cell adhesion and actin cytosqueleton				
P27870/ VAV_MOUSE	Vav1	Proto-oncogene vav	**3.09** [b] p=N/A	**3.237** [b] p=N/A
Q9JKK7/ TMOD2_MOUSE	Tmod2	Tropomodulin-2	**0.413** [a] p=0.01508	**0.626** [a] p=0.04263
P47226/ TES_MOUSE	Tes	Testin	**1.883** [a] p=0.04618	1.457 * p=0.1128
Maintenance of mitocondrial structure				
Q8CAQ8/ IMMT_MOUSE	Immt	MICOS complex subunit Mic60	**0.383** [a] p=0.003721	**0.519** [a] p=0.005439

[a] Fold changes in bold and underlined were assigned by MASCOT as a statistically significant change considering three or more identified peptides, the normality test was successful, and their corresponding p values lower than 0.05.

[b] Fold changes in bold and underline with a p=N/A means a statistically significant fold changes that the quantitation is supported only by one or two peptides. The p value was not assigned because the individual peptide are contained in OFFGEL fractions that do not have a normal distribution. If the fold change value is not written in bold and underlined means it does not pass the normality test of MASCOT.

[c] Fold changes with a non-calculated p value (p= —) were those that did not follow a normal distribution and all the individual peptides supporting the quantification are contained in fractions that do not satisfied the normal distributions.

[d] Fold changes written in italics and followed by a parenthesis indicating a fraction number (F1–F12), indicates proteins that did not pass the normality test of MASCOT but the p value was calculated based on the detection of one derived peptide in one OFFGEL fraction that has a normal distribution.

[e] Fold changes labeled with asterisks are those with p values higher than 0.05.

[f] Statistically significant up- and down-regulated proteins were considered those with fold change values lower than 0.60 and higher 1.50, respectively for which MASCOT assigned a p value lower than 0.05.

peptide treatment in the activation of J774 cells.

3.1. A233 treatment increases superoxide anion levels in J774.2 cells

Peptide treatment increases $O_2^{\bullet -}$ (superoxide anion) levels in tilapia head–kidney leukocyte cultures [2]. Together, the GO biological process and the molecular function enrichment analyses indicate an impact on oxidation–reduction processes after 6 h of treatment, with the differential up-regulation of superoxide dismutase Sod1 and Prdx6 peroxidase (Fig. 1, Supplemental Table 2). Prdx6 is primarily a phospholipid peroxidase that protects membranes from oxidation and is considered to be a cytoprotective enzyme; it also contains phospholipase A2 activity required for the activation of NADPH oxidase NOX2, and thus for ROS generation [20,21].

Activated M1 macrophages mediate their cytotoxic and pro-inflammatory effects by producing ROS and RNS such as $O_2^{\bullet -}$ and NO (nitric oxide), respectively [22]. ROS generation induces cell damage, for example, by reacting with NO to yield $ONOO^-$ (peroxynitrite anion) [23]. Sod1 and Prdx6 up-regulation might then suggest an increase in ROS production, while avoiding associated oxidative stress damage. Correspondingly, the effect of the GHS A233 and GHRP-6 on $O_2^{\bullet -}$ production was determined, demonstrating a significant increase of $O_2^{\bullet -}$ levels compared with the control in both cases (Fig. 2). Therefore, A233 treatment might potentiate macrophage activation and cytotoxic functions, as ROS production has been reported to have role in macrophage differentiation [24].

3.2. A233 treatment differentially modulates DNA repair and apoptosis related proteins

Activated macrophages are protected against ROS induced oxidative damage by showing, for instance, an enhancement of DNA repair and resistance to apoptosis [25]. Apoptosis is an ordered cascade of enzymatic events that culminates in cell death and the cleavage of DNA into characteristic nucleosomal fragments. Since peptide treatment increases $O_2^{\bullet -}$ levels, we investigated the modulation of these events. The GO biological process enrichment analysis highlighted the differential up-regulation of DNA repair proteins at 6 and/or 12 h post-treatment (Fig. 1, Supplemental Table 2). For example, the differentially modulated protein Nabp1 is a component of the SOSS complex required for efficient homologous recombination-dependent repair of double-strand breaks and ATM-dependent signaling pathways [26,27]. Therefore, these findings indicate that DNA repair enhancement and resistance to apoptosis in J774.2 cells might be potentiated by A233 peptide treatment, which might promote survival under conditions with high-ROS levels.

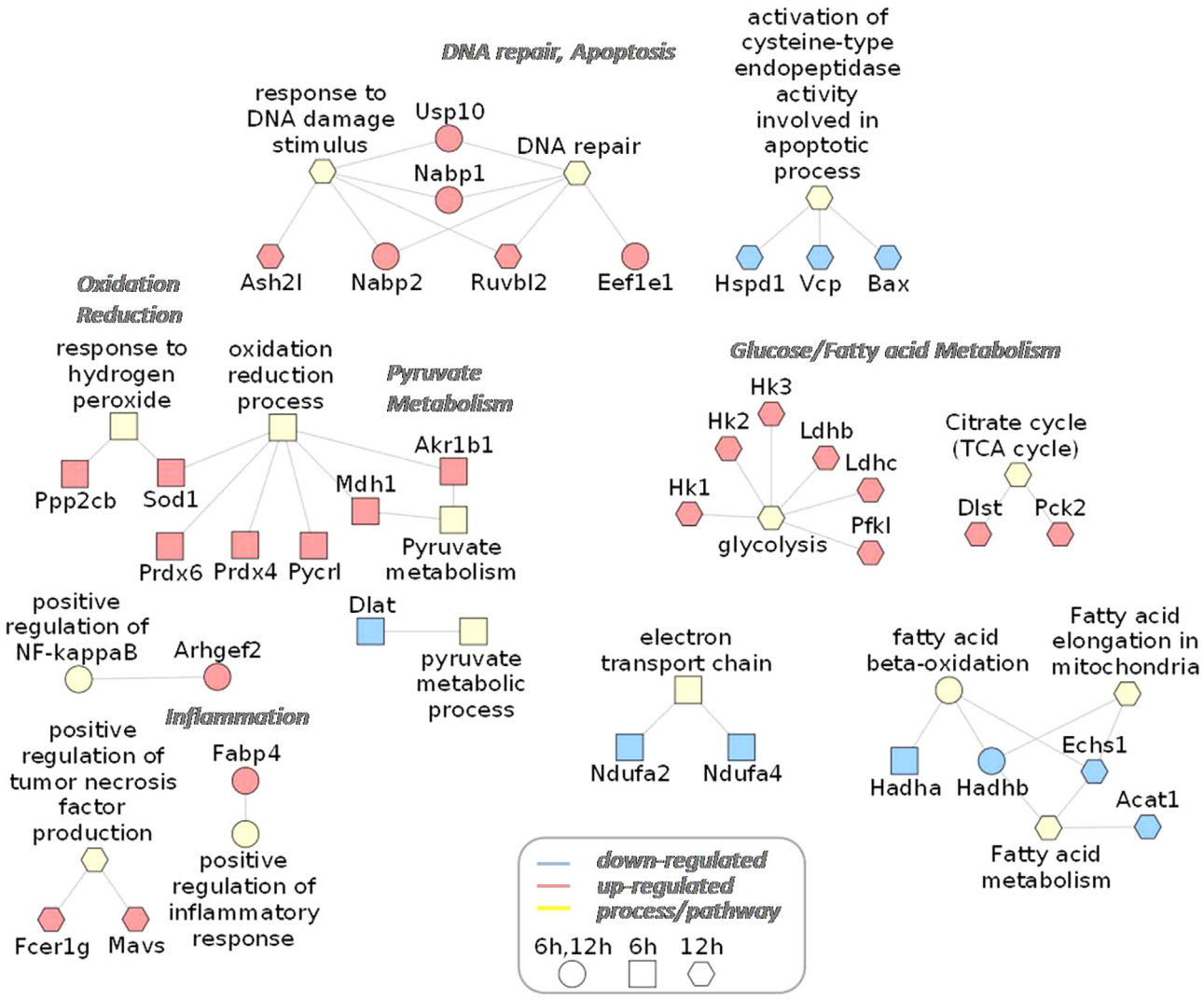

Fig. 1. GO biological process and KEGG pathway enrichment analyses of the differentially modulated proteins at 6 and/ or 12 h of treatment with A233 peptide.

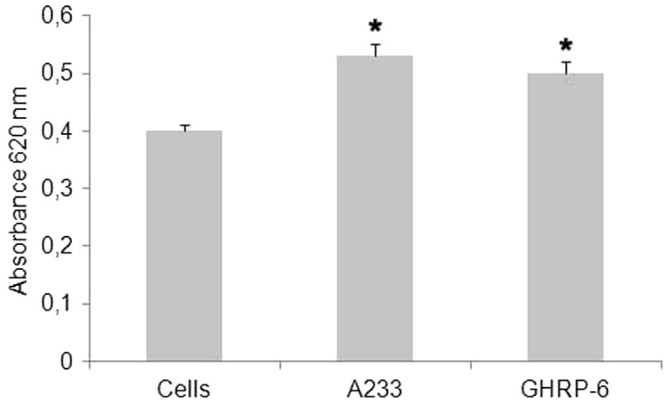

Fig. 2. Superoxide anion production in macrophage J774 cells stimulated with A233 peptide. Cells were incubated with the A233 and GHRP-6 peptides for 4 h at 37 °C in 5% CO_2; control cells were treated with Hanks' solution (pH 7.4). Data are expressed as the absorbance at 620 nm. Statistical significance between groups was determined using one-way ANOVA with Newman–Keuls's test (*: $p < 0.05$). The results are representative of two independent experiments.

3.3. A233 treatment differentially modulates STAT1 target proteins

The activation of the transcription factors NF-κB, STAT1 and AP-1 by stimuli like LPS, and/or IFN-α/β/γ induces the expression of inflammatory and microbicidal M1 genes. To investigate their activation in the A233 peptide-stimulated cells, we conducted a TFBS enrichment analysis at 6 and 12 h post-treatment and at each time separately. Noticeably, we detected a significant enrichment of the STAT1 targets at 6 and/or 12 h post-treatment, including Eef1g, Fabp4, Hadhb, Hk3, yar, Mcm3, Phb, Ptcd3,and Rtn3 (Supplemental Table 2).

In particular, the differentially up-regulated protein Fabp4 (Fig. 1, Table 1) is a target gene of the STAT1 transcription factor (Supplemental Table 2). The expression of Fabp4 in macrophages is induced by a pro-inflammatory environment, and its decrease reduces NF-κB activation and the levels of the inflammatory cytokines Cox2 and iNOS [29,30]. This protein also displays an antioxidant activity against H_2O_2 in vitro [31]. The increase in Fabp4 protein may thus link peptide treatment with the establishment of a pro-inflammatory phenotype by responding to STAT1 and inducing NF-κB activation.

3.4. A233 treatment increases IFN-γ levels and induces an antiviral response

As suggested by the TFBS enrichment analysis, the A233 peptide may activate the STAT1 signaling pathway. IFN-γ polarizes macrophages to an M1 state through STAT1 activation, while deletion of STAT1 compromises viral immunity [32]. Activated STAT1

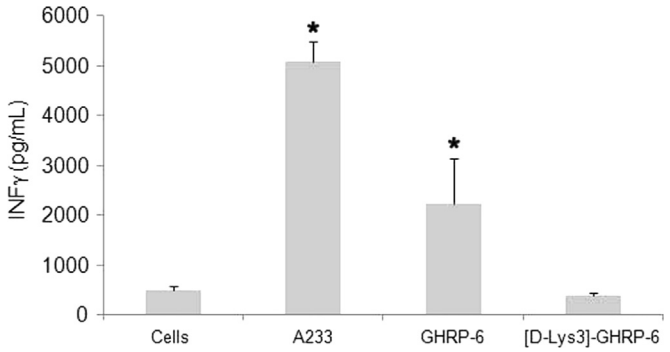

Fig. 3. IFN-γ production in mouse splenocytes stimulated with A233 peptide (10 nM). The levels of IFN-γ were measured by ELISA in the cell supernatant after four days of stimulation. The GHRP-6 and [D-Lys$_3$]-GHRP-6 were included as positive and negative peptide controls, respectively. Data represent mean ± standard error of the mean (SEM); $N=5$. Statisitical analysis was performed by a one-way analysis of variance, using Newman–Keuls post-test. (*: $p<0.05$). The results are representative of two independent experiments.

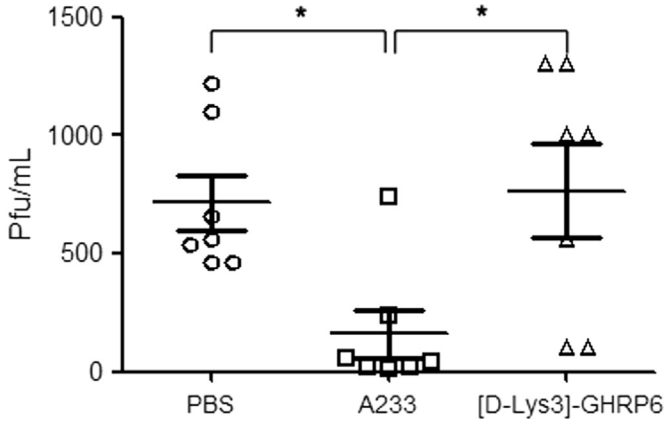

Fig. 4. DENV load in mouse brain after treatment with A233 peptide and virus challenge. DENV was detected in brain samples collected 7 days after challenge of treated mice by direct quantification on Vero cells. Data represent mean ± standard error of the mean (SEM); $N=7$. Statistical analysis was performed by one-way analysis of variance, using Kruskal–Wallis and Dunn multiple comparison test. (*: $p<0.05$). The results are representative of two independent experiments.

is transported to the nucleus, where it induces the expression of ROS-generating enzymes, iNOS and pro-inflammatory cytokines [33]. Therefore, we measured IFN-γ levels in mouse splenocytes stimulated with the peptide. As suspected, A233 treatment significantly increased IFN-γ levels (5099.73 ± 86.16 pg/mL) compared to the control cells (558.05 ± 26.48 pg/mL). Also, the stimulation with the antagonist peptide [D-Lys^3]-GHRP6 induced a low cytokine secretion (430.45 ± 7.22 pg/mL) (Fig. 3).

Considering that this cytokine is a mediator of antiviral activity against DENV [34], we evaluated the antiviral capacity of A233 peptide in a mouse model of DENV infection. This model, based on the intracranial inoculation of high viral doses of mouse-adapted strains, has previously been used to evaluate the efficacy of antiviral drugs against DENV [35,36]. Our results reveal a significant reduction in viral load in treated mice after intracranial challenge with DENV-3 (161.43 ± 29.71 pfu/mL), compared with the control group (714.29 ± 34.87 pfu/mL) (Fig. 4). A similar outcome was observed after challenge with the DENV-2 NGC strain (data not shown). The administration of an antagonist [D-Lys^3]-GHRP-6 peptide did not reduce viral load after challenge (765.71 ± 57.54 pfu/mL) (Fig. 4). Further experiments could be conducted in mice and non-human primates to evaluate the efficacy of the molecule against infectious and non-infectious diseases.

On the other hand, peptide treatment of J774.2 cells differentially up-regulates the peroxisomal and mitochondrial protein MAVS required for innate immune defense against viruses (Fig. 1, Table 1). The mitochondrial isoform of MAVS activates an IFN-dependent signaling pathway that amplifies and stabilizes the antiviral response through the expression of type I IFNs and of other antiviral cytokines [37]. The differential up-regulation of MAVS, the increase in IFN-γ levels, and the protection against DENV infection indicates an anti-viral effect of A233 peptide treatment. Other mouse model studies examining mechanisms of antiviral innate immunity against DENV reveal an essential role for MAVS [38] and IRF-3/7 [39].

4. Conclusion

The present study shows that A233 peptide treatment stimulates $O_2^{\bullet-}$ and IFN-γ production in mouse J774.2 macrophages and splenocytes, respectively. IFN-γ can polarize macrophages to the M1 classically active state. The proteomic profiling of J774.2 cells stimulated with the A233 peptide indicated an up-regulation of glycolytic pathway proteins and the down-regulation of fatty acid beta-oxidation and oxidative phosphorylation proteins, which may correspond to a shift from aerobic to anaerobic glucose catabolism. It also suggested the adaptation of J774.2 cells to the increase of $O_2^{\bullet-}$ levels through the up-regulation of antioxidant enzymes and of double-stranded DNA break repair proteins and the down-regulation of the pro-apoptotic protein Bax. In addition, it pointed to the induction of an antiviral state reflected by increased IFN-γ levels in mouse splenocytes and the differential modulation of MAVS protein. This effect was assessed in a mouse model of intracranial dengue virus infection, and the A233 peptide was shown to decrease viral load after challenge. Altogether, peptide treatment may positively regulate pathogen killing by macrophages, which is supported at the molecular level by the increase in $O_2^{\bullet-}$ and IFN-γ. Further studies should be performed to further test and extend these findings.

The iTRAQ data shown in our manuscript should be considered as preliminary results that should be further validated by additional proteomics experiments with greater statistical power as well as by using orthogonal techniques such as western-blotting or ELISA.

Acknowledgments

The authors would like to appreciate Dr Eva Harris, Professor, Division of Infectious Diseases and Vaccinology Director, Center for Global Public Health UC Berkeley and Dr. John van der Meer for their precious help in the manuscript revision

Appendix A

Transprancy document associated with this article can be found in the online version at http://dx.doi.org/10.1016/j.bbrep.2016.01.008.

References

[1] S. Unniappan, R.E. Peter, Structure, distribution and physiological functions of ghrelin in fish, Comp. Biochem. Physiol. A. Mol. Integr. Physiol. 140 (2005) 396–408.

[2] R. Martinez, K. Ubieta, F. Herrera, A. Forellat, R. Morales, A. de la Nuez, R. Rodriguez, O. Reyes, A. Oliva, M.P. Estrada, A novel GH secretagogue, A233, exhibits enhanced growth activity and innate immune system stimulation in teleosts fish, J. Endocrinol. 214 (2012) 409–419.

[3] V.D. Dixit, E.M. Schaffer, R.S. Pyle, G.D. Collins, S.K. Sakthivel, R. Palaniappan, J. W. Lillard, D.D. Taub, Ghrelin inhibits leptin- and activation-induced proinflammatory cytokine expression by human monocytes and T cells, J. Clin. Invest. 114 (2004) 57–66.
[4] T. Waseem, M. Duxbury, H. Ito, S.W. Ashley, M.K. Robinson, Exogenous ghrelin modulates release of pro-inflammatory and anti-inflammatory cytokines in LPS-stimulated macrophages through distinct signaling pathways, Surgery 143 (2008) 334–342.
[5] K. Bujold, D. Rhainds, C. Jossart, M. Febbraio, S. Marleau, H. Ong, CD36-mediated cholesterol efflux is associated with PPARgamma activation via a MAPK-dependent COX-2 pathway in macrophages, Cardiovasc. Res. 83 (2009) 457–464.
[6] A. Demers, A. Rodrigue-Way, A. Tremblay, Hexarelin Signaling to PPARgamma in Metabolic Diseases, PPAR Res. 2008 (2008) 364784.
[7] S.K. Biswas, A. Mantovani, Orchestration of metabolism by macrophages, Cell. Metab. 15 (2012) 432–437.
[8] A. Mantovani, A. Sica, S. Sozzani, P. Allavena, A. Vecchi, M. Locati, The chemokine system in diverse forms of macrophage activation and polarization, Trends Immunol. 25 (2004) 677–686.
[9] F.O. Martinez, S. Gordon, The M1 and M2 paradigm of macrophage activation: time for reassessment, F1000Prime Rep. 6 (2014) 13.
[10] T. Yada, H. Kaiya, K. Mutoh, T. Azuma, S. Hyodo, K. Kangawa, Ghrelin stimulates phagocytosis and superoxide production in fish leukocytes, J. Endocrinol. 189 (2006) 57–65.
[11] L. Gil, E. Marcos, A. Izquierdo, L. Lazo, I. Valdés, P. Ambala, L. Ochola, R. Hitler, E. Suzarte, M. Álvarez, P. Kimiti, J. Ndung'u, T. Kariuki, M.G. Guzmán, G. Guillén, L. Hermida, The protein DIIIC-2, aggregated with a specific oligodeoxynucleotide and adjuvanted in alum, protects mice and monkeys against DENV-2, Immunol. Cell. Biol. 93 (2015) 57–66.
[12] M. Magrane, U. Consortium, UniProt Knowledgebase: a hub of integrated protein data, Database (Oxford). 2011 (2011), bar009.
[13] A. Doms, M. Schroeder, GoPubMed: exploring PubMed with the Gene Ontology, Nucleic Acids Res. 33 (2005) W783–W786.
[14] C.L. Smith, J.T. Eppig, The mammalian phenotype ontology: enabling robust annotation and comparative analysis, Wiley Interdiscip. Rev. Syst. Biol. Med., 1 (n.d.), 2009, 390–399.
[15] D. Tabas-Madrid, R. Nogales-Cadenas, A. Pascual-Montano, GeneCodis3: a non-redundant and modular enrichment analysis tool for functional genomics, Nucleic Acids Res. 40 (2012) W478–W483.
[16] K. Breuer, A.K. Foroushani, M.R. Laird, C. Chen, A. Sribnaia, R. Lo, G.L. Winsor, R. E.W. Hancock, F.S.L. Brinkman, D.J. Lynn, InnateDB: systems biology of innate immunity and beyond–recent updates and continuing curation, Nucleic Acids Res. 41 (2013) D1228–D1233.
[17] Y. Wang, R. Thilmony, Y.Q. Gu, NetVenn: an integrated network analysis web platform for gene lists, Nucleic Acids Res. 42 (2014) W161–W166.
[20] A.B. Fisher, Peroxiredoxin 6: a bifunctional enzyme with glutathione peroxidase and phospholipase A_2 activities, Antioxid. Redox Signal. 15 (2011) 831–844.
[21] S. Chatterjee, S.I. Feinstein, C. Dodia, E. Sorokina, Y.-C. Lien, S. Nguyen, K. Debolt, D. Speicher, A.B. Fisher, Peroxiredoxin 6 phosphorylation and subsequent phospholipase A2 activity are required for agonist-mediated activation of NADPH oxidase in mouse pulmonary microvascular endothelium and alveolar macrophages, J. Biol. Chem. 286 (2011) 11696–11706.
[22] Y. Xia, J.L. Zweier, Superoxide and peroxynitrite generation from inducible nitric oxide synthase in macrophages, Proc. Natl. Acad. Sci. USA 94 (1997) 6954–6958.
[23] C. Szabó, B. Zingarelli, M. O'Connor, A.L. Salzman, DNA strand breakage, activation of poly (ADP-ribose) synthetase, and cellular energy depletion are involved in the cytotoxicity of macrophages and smooth muscle cells exposed to peroxynitrite, Proc. Natl. Acad. Sci. USA 93 (1996) 1753–1758.
[24] A. Covarrubias, V. Byles, T. Horng, ROS sets the stage for macrophage differentiation, Cell. Res. 23 (2013) 984–985.
[25] M. Bauer, M. Goldstein, M. Christmann, H. Becker, D. Heylmann, B. Kaina, Human monocytes are severely impaired in base and DNA double-strand break repair that renders them vulnerable to oxidative stress, Proc. Natl. Acad. Sci. USA 108 (2011) 21105–21110.
[26] J. Huang, Z. Gong, G. Ghosal, J. Chen, SOSS complexes participate in the maintenance of genomic stability, Mol. Cell 35 (2009) 384–393.
[27] E.A. Nam, D. Cortez, SOSS1/2: sensors of single-stranded DNA at a break, Mol. Cell. 35 (2009) 258–259.
[29] L. Makowski, K.C. Brittingham, J.M. Reynolds, J. Suttles, G.S. Hotamisligil, The fatty acid-binding protein, aP2, coordinates macrophage cholesterol trafficking and inflammatory activity Macrophage expression of aP2 impacts peroxisome proliferator-activated receptor gamma and IkappaB kinase activities, J. Biol. Chem. 280 (2005) 12888–12895.
[30] K. Kajimoto, Y. Minami, H. Harashima, Cytoprotective role of the fatty acid binding protein 4 against oxidative and endoplasmic reticulum stress in 3T3-L1 adipocytes, FEBS Open. Bio 4 (2014) 602–610.
[31] J.E. Durbin, R. Hackenmiller, M.C. Simon, D.E. Levy, Targeted disruption of the mouse Stat1 gene results in compromised innate immunity to viral disease, Cell 84 (1996) 443–450.
[32] A. Sica, A. Mantovani, Macrophage plasticity and polarization: in vivo veritas, J. Clin. Invest. 122 (2012) 787–795.
[33] S. Shresta, J.L. Kyle, H.M. Snider, M. Basavapatna, P.R. Beatty, E. Harris, Interferon-dependent immunity is essential for resistance to primary dengue virus infection in mice, whereas T- and B-cell-dependent immunity are less critical, J. Virol. 78 (2004) 2701–2710.
[34] P.H. Huang, F.M. White, Phosphoproteomics: unraveling the signaling web, Mol. Cell. 31 (2008) 777–781.
[35] J.-C. Lee, S.-J. Won, C.-L. Chao, F.-L. Wu, H.-S. Liu, P. Ling, C.-N. Lin, C.-L. Su, Morusin induces apoptosis and suppresses NF-kappaB activity in human colorectal cancer HT-29 cells, Biochem. Biophys. Res. Commun. 372 (2008) 236–242.
[36] T. Ohman, J. Rintahaka, N. Kalkkinen, S. Matikainen, T.A. Nyman, Actin and RIG-I/MAVS signaling components translocate to mitochondria upon influenza A virus infection of human primary macrophages, J. Immunol. 182 (2009) 5682–5692.
[37] S.T. Perry, T.R. Prestwood, S.M. Lada, C.A. Benedict, S. Shresta, Cardif-mediated signaling controls the initial innate response to dengue virus in vivo, J. Virol. 83 (2009) 8276–8281.
[38] H.W. Chen, K. King, J. Tu, M. Sanchez, A.D. Luster, S. Shresta, The roles of IRF-3 and IRF-7 in innate antiviral immunity against dengue virus, J. Immunol. 191 (2013) 4194–4201.
[39] D. Augustyniak, J. Nowak, F.T. Lundy.2012, Direct and indirect activities of neuropeptides and their therapeutic potential, Curr. Protein Pept. Sci. 13 (2012) 723–738.